

Modellering van geulen, platen en drempels in de Westerschelde ¹

projectnummer: RKZ-536
projectleider: Drs. H. Verbeek

Faserapport 1

**One-dimensional long-term equilibria of tidal
embayments**

(met een Nederlandse samenvatting)

H.M. Schuttelaars

¹Dit project is uitgevoerd in opdracht van het Rijksinstituut voor Kust en Zee te Middelburg

OPDRACHTGEVER:	Rijksinstituut voor Kust en Zee van het Directoraat Generaal Rijkswaterstaat Middelburg
TITEL:	Modellering van geulen, platen en drempels in de Westerschelde
<p data-bbox="411 645 683 678">SAMENVATTING:</p> <p data-bbox="411 741 1337 898">In dit project zal een geïdealiseerd, nietlineair model worden ontwikkeld voor een estuarium met karakteristieken als die van de Westerschelde, teneinde het dynamisch gedrag van geulen en zandplaten te onderzoeken. Daarbij ligt de nadruk op het analyseren van fysische mechanismen, die aanleiding geven tot een aantal specifieke karakteristieken, nl.</p> <ul data-bbox="453 922 1337 1090" style="list-style-type: none"> • meandergedrag van geulen • het cyclisch gedrag van kortsluitgeulen, die de verbinding vormen tussen de hoofdgeulen • de vorming van zogeheten drempels <p data-bbox="411 1149 927 1176">Het onderzoek bestaat uit een drietal fasen:</p> <ul data-bbox="453 1202 1337 1433" style="list-style-type: none"> • Verkenning Westerschelde en experimenten met een 1D model. • Vergelijking uitkomsten 1D model met beschikbare veldgegevens en numerieke modellen en numerieke modellen, alsmede lineaire stabiliteitsanalyse van het 2D model. • Vergelijking uitkomsten 2D model met beschikbare veldgegevens en numerieke modellen, alsmede niet-lineaire experimenten met het 2D model. <p data-bbox="411 1462 1155 1489">In dit rapport zijn de bevindingen uit de eerste fase vastgelegd.</p>	

Inhoudsopgave

Nederlandse Samenvatting	Introduction	13
2	Model Description	15
3	Scaling and Expansion	16
4	The Short Embayment Regime	19
5	Numerical Experiments	20
5.1	No Overtides	20
5.2	Overtides, no phase difference	25
6	Conclusions	29
A	Dependence of resonance length on bed profile and frictional strength	30
B	Frictional Length Scale	32
C	The Moving Boundary	34
C.1	Boundary Conditions at the Moving Boundary	34
C.2	Boundary Conditions at a Fixed Space Coordinate	35
D	Closure of the Eastern Scheldt	36

Lijst van figuren

1	The marine salt and brackish part of the Western Scheldt estuary from Vlissingen to Antwerp.	13
2	Cross-sectional view of the embayment.	15
3	Analytical (no λ_V^2 corrections) and numerical equilibrium bed profiles are plotted for an embayment with length $L = 2 \cdot 10^4$ m. The parameters used are given in table 2.	20
4	Contour plot of the equilibrium bed profile for different embayment lengths as a function of x/L . Here $L_g \sim 550$ km. The system is only forced with an externally prescribed M_2 -tide. . .	21
5	Contour plots of the amplitude and phase of the M_2 and M_4 horizontal tide as a function of embayment L/L_g and x/L . The velocities are scaled with the characteristic velocity \sqrt{gH}	23
6	Contour plots of the leading order sediment fluxes as function of the scaled embayment length L/L_g and x/L . Here $L_g = 2\pi\sqrt{gH}/\sigma \sim 550$ km and $\beta = 0.0$ for the equilibrium bed profile as shown in figure 4. The amplitudes of the fluxes are scaled with $(\alpha/\gamma)(\epsilon\sqrt{gH})^3$	24
7	Contour plot of the equilibrium bed profile as function of the scaled embayment length L/L_g and x/L . Here $L_g = 2\pi\sqrt{gH}/\sigma \sim 550$ km, $\beta = 0.05$ and $\phi = 0^\circ$. The depth at the entrance of the embayment is 15 m.	26
8	Contour plots of the amplitude and phase of the M_2 , internally generated and externally prescribed M_4 horizontal velocity profile as function of the scaled embayment length L/L_g and x/L . Here $L_g = 2\pi\sqrt{gH}/\sigma \sim 550$ km, $\beta = 0.05$ and $\phi = 0^\circ$. The amplitudes of the velocity are scaled with \sqrt{gH}	27
9	Contour plots of the leading order sediment fluxes as function of the scaled embayment length L/L_g and x/L . Here $L_g = 2\pi\sqrt{gH}/\sigma \sim 550$ km, $\beta = 0.05$ and $\phi = 0^\circ$ for the equilibrium bed profile as shown in figure 7. The amplitudes of the fluxes are scaled with $(\alpha/\gamma)(\epsilon\sqrt{gH})^3$	28
10	In this figure the resonance length compared to the tidal wave length $2\pi\sqrt{gH}/\sigma$, is plotted for different bed profiles (different α 's, where $h(x) = 1 - (1 - x)^\alpha$) and different values of drag coefficient C_D . Note that due to both friction and a depth dependent bed profile the resonance length becomes shorter.	32
11	In this figure the amplitude of the vertical tide at the end of the embayment is plotted for two values of the drag coefficient C_D . For C_D small enough, more than one resonance length (with the length compared to the tidal wave length $2\pi\sqrt{gH}/\sigma$) is observed, if C_D is increased, only one resonance length is retained. Here $\alpha = 0$, but this observation is still valid for $\alpha > 0$	32

- 12 The equilibrium profiles for the Eastern Scheldt before and after the building of the storm surge. The embayment length $L = 45$ km, its depth at the entrance $H = 20$ m and its width 8 km. The area between the two equilibria is the total amount of sediment that has to be imported by the system to be able to reach this new equilibrium. Using this figure it is estimated to be $231 \times 10^6 \text{ m}^3$ of sediment. 36

Nederlandse samenvatting

Algemeen kader

Veel zeegaten en estuaria worden gekenmerkt door wisselwerkingen tussen de waterbeweging (geforceerd door getijden, wind, golven en dichtheidsverschillen), het transport van sediment en morfologische veranderingen. Dit resulteert in bodempatronen bestaande uit geulen afgewisseld door platen, die een sterke dynamiek vertonen, zowel in de ruimte als in de tijd.

Voor een effectief beheer van dergelijke gebieden is het noodzakelijk om kwantitatieve voorspellingen te kunnen maken van waterstanden, stromingen, transportprocessen en bodemontwikkelingen. Deze informatie is relevant voor dijkbescherming, routing van schepen, verspreiding van stoffen, ecologische toepassingen, etc.. Een gedeelte van de huidige generatie modellen is goed bruikbaar voor het maken van korte-termijn voorspellingen (tijdschaal dagen-weken). Andere modellen, gebaseerd op empirische relaties voor morfodynamisch evenwicht, gecombineerd met hydrodynamische en sediment modules gebaseerd op fysische wetten, zoals ESTMORF en EENDMORF (Fokkink, 1998), of geheel gebaseerd op fysische wetten (De Jong, 1998) zijn wel in staat tot lange termijnsvoorspellingen. Deze laatste klasse van modellen is één dimensionaal. Het is dus nog niet mogelijk om bijvoorbeeld het drie dimensionale gedrag van geulen en platen te simuleren over een periode van maanden tot jaren. Een belangrijke oorzaak hiervoor is de beperkte kennis van fysische processen (met name turbulente uitwisselingsprocessen en het transport van sediment). Dit kan leiden tot snelle foutengroei, met name in getijdebekken, immers de morfologie in zulke gebieden wordt bepaald door divergenties in kleine netto transporten, die het verschil zijn tussen de grote transporten gedurende de eb- en vloedperiode. Ook het beschrijven van de terugkoppeling van bodem naar de waterbeweging geeft aanleiding tot problemen, vooral in ondiepe gedeelten. Een hiermee samenhangend probleem is dat het nog onduidelijk is welke fysische processen van wezenlijk belang zijn voor morfologisch gedrag op tijdschalen waar de terugkoppeling van bodem naar de waterbeweging essentieel is. Daarnaast is er nog onvoldoende kennis omtrent de inherente dynamische eigenschappen van morfologische systemen. Zo zijn er aanwijzingen dat, onder bepaalde omstandigheden, de interne dynamica resulteert in explosieve foutengroei, met als gevolg dat het systeem een voorspelbaarheidshorizon heeft.

Specifieke doelstelling onderzoeksproject

De hierboven genoemde problematiek vormt het algemene kader van het huidige onderzoeksproject, dat wordt uitgevoerd in opdracht van het RIKZ Middelburg door het IMAU (universiteit Utrecht). De nadruk ligt hierbij op een specifiek estuarium, namelijk de Westerschelde, zie figuur 1. Dit bekken is economisch van groot belang omdat het de scheepvaartroute naar de haven van Antwerpen is. Daarnaast heeft het gebied een grote ecologische waarde. Uitgangspunt van het beheer is het garanderen van de scheepvaart met behoud van de natuurlijke

waarde van het estuarium. De afgelopen jaren heeft dit tot problemen geleid: baggeractiviteiten (zo'n $8 \times 10^6 \text{m}^3/\text{jr}$) en verdieping van de vaargeul hebben gezorgd voor verminderde activiteit van geulen en platen in het bekken; de vraag vanuit het beheer is of en hoe deze negatieve effecten kunnen worden voorkomen.

De doelstellingen van dit onderzoek zijn

- Het vaststellen of er morfodynamische evenwichten bestaan.
- Het bekijken van de stabiliteit van deze evenwichten.
- Het lange termijngedrag van geulen en platenstelsels bestuderen.
- Het onderzoeken van de gevoeligheid van evenwichten op ingrepen.

Teneinde deze vragen te beantwoorden wordt er een geïdealiseerd model ontwikkeld. Dit model bevat de essentiële fysica en is nog eenvoudig genoeg om met mathematische methoden te analyseren.

De Westerschelde

De totale lengte van de Westerschelde bedraagt zo'n 160km (tot Gent); in het mariene gedeelte (de eerste 60 km) neemt de breedte van het bekken langzaam af van 5km naar enkele honderden meters. Waterdiepten in de geulen variëren van 25m nabij Vlissingen tot 50m nabij Borssele en nemen dan af richting Antwerpen. De waterbeweging in het bekken wordt gedomineerd door het dubbeldaagse zon- en maansgetij; de amplitude van de waterstanden bedraagt ongeveer 2m nabij Vlissingen en neemt het bekken in toe ($\pm 2.5\text{m}$ nabij Antwerpen), karakteristieke stroomsnelheidsamplituden bedragen ongeveer 1m/s. De waargenomen faseverschuiving in landwaartse richting duidt op een gedeeltelijk gereflecteerde getijgolf. Ten gevolge van de traagheid van de waterbeweging, bodemwrijving en massabehoud worden hogere harmonischen van het basisgetij opgewekt (met name de M_4 -component en in mindere mate de M_6 component), alsmede residuele stromingen. Dit resulteert in intern gegenereerde asymmetrie van zowel het verticale- als het horizontale getij. Daarnaast bestaat er ook extern opgelegde asymmetrie als gevolg van de door de Noordzee opgelegde M_2 - en M_4 -getijcomponenten aan de zeevaartse rand van het bekken. De uitstroom van de Schelderivier bedraagt gemiddeld $100 \text{m}^3/\text{s}$, hetgeen klein is (ongeveer 1% op de Nederlands-Belgische grens) ten opzichte van de getijfluxen.

De door de waterbeweging geïnduceerde bodemschuifspanningen zijn voldoende groot om sediment op te werfelen en te transporteren. Het grootste gedeelte van het materiaal bestaat uit fijn zand (korrelgrootte ongeveer 0.2 mm), dat wordt getransporteerd als zwevend stof. Ten gevolge van met name getijasymmetrie, reststromingen en 'settling lag' effecten ontstaan netto transporten, die bepalend zijn voor de morfologie. Met settling lag wordt bedoeld dat er een faseverschil is tussen de concentratie van gesuspendeerd materiaal en de stroomsnelheid omdat deeltjes enige tijd nodig hebben om uit te zakken.

De morfologie van de Westerschelde wordt gekenmerkt door een aantal hoofd-geulen, waarvan het aantal afneemt van drie aan de zeevaartse zijde tot 1 dieper

in het bekken. Er blijkt een duidelijk verschil tussen ebgeulen (getijgemiddeld transport van water zeewaarts gericht) en vloedgeulen. De eerstgenoemden vertonen meandergedrag, met een kenmerkende lengteschaal van 5km, terwijl de laatsten meer recht zijn. Op de overgang tussen twee bochten bevinden zich drempels, dat wil zeggen locaties waar netto sedimentatie optreedt. De hoofdgeulen zijn onderling verbonden door zogeheten kortsluitgeulen, die cyclisch gedrag blijken te vertonen in ruimte en tijd. Verder worden in bepaalde gebieden van het bekken, zoals in het Verdrongen Land van Saafdinghe, fractale patronen van geulen waargenomen.

Het model

Teneinde de fundamentele kennis van het morfologische gedrag van de Westerschelde te vergroten is een geïdealiseerd model van dit bekken ontwikkeld. Een groot voordeel van zo'n model is dat slechts een beperkt aantal fysische processen expliciet wordt beschreven, zodat het transparant is en kan worden geanalyseerd met behulp van wiskundige methoden. Vergelijkbare modellen zijn hiervoor ontwikkeld voor de korte bekkens in de Waddenzee en zijn zeer succesvol omdat ze een verklaring gaven voor waargenomen gedrag. Voorbeelden zijn de geobserveerde bodemprofielen, bekende empirische relaties (zoals een ruimtelijk uniforme bodemschuifspanning), het netto importeren van sediment na een gedeeltelijke afsluiting (Friese Zeegat), het ontstaan en splitsen van geulen en het migratiegedrag van platen aan de zeewaartse kant van de bekkens.

Het model voor de Westerschelde verschilt op een aantal wezenlijke punten van die voor korte bekkens. In de eerste plaats betreft het hier een lang bekken, zodat er sprake is van een ruimtelijk niet-uniforme getij. Dit heeft tevens als consequentie dat bodemwrijving een cruciale rol speelt in de dynamica van de waterbeweging. Tevens is de rol van traagheid essentieel, waardoor getij-asymmetrie en reststromen ontstaan en het dominante transport van sediment op de getijdetijdschaal wordt bepaald door advectione processen. Aangezien korte bekkens het bestaan van morfologische evenwichten toelaten is als eerste onderzocht of het Westerscheldemodel morfodynamische evenwichten toelaat en zo ja, wat zijn hun eigenschappen en welke fysische processen bepalen de sedimentbalans?

Het domein van het model is een rechthoekig bekken met niet-erodeerbare zijwanden en aan de landwaartse zijde is de waterdiepte nul, zie figuur 2. De bewegingsvergelijkingen bestaan uit de één-dimensionale ondiepwatervergelijkingen, waarin de bodemschuifspanning is gelineariseerd volgens het Lorentz-principe. Daaraan zijn toegevoegd een vergelijking voor de breedtegemiddelde en diepte-geïntegreerde concentratie, inclusief opwerveling- en depositietermen, en een bodemevolutievergelijking. Als randvoorwaarden wordt op de zeewaartse rand het verticale getij voorgeschreven (zowel een M_2 - als M_4 -component) en de bodem vastgehouden. Aan de landwaartse kant wordt de netto sedimentflux (bestaande uit een advectioneel en diffusief deel) nul gesteld. Tot slot worden geen diffusieve grenslagen in het tijdosillerende deel van de concentratie toegestaan. Het eerste belangrijke verschil met een eerder model, ontwikkeld door

Karin de Jong, is dat hier geen rivieruitstroom wordt meegenomen. In plaats daarvan kunnen advectione fluxen worden gecompenseerd door diffusieve fluxen, waardoor wel grenslagen in de gemiddelde concentratie ontstaan. Een tweede verschil is dat hier intern gegenereerde getij-asymmetrie expliciet wordt meegenomen; in het model van de Jong is er alleen sprake van extern opgelegde getij-asymmetrie. Tot slot wordt in het hier besproken model de dwarsdoorsnede van het bekken constant verondersteld, terwijl dit in het andere model ruimtelijk varieert. Teneinde de modellen op dit punt te kunnen vergelijken kan, bij een gegeven modelbodem, een actuele dwarsdoorsnede worden berekend door de waterdiepte te vermenigvuldigen met de actuele breedte.

Analyse en resultaten

Het model is allereerst dimensieloos gemaakt door gebruik te maken van relevante ruimte- en tijdschalen. Belangrijk daarbij is dat de morfologische tijdschaal veel groter is dan de getijperiode en wrijvingstijdschaal. Dit leidt tot een dimensieloze wrijvingscoëfficiënt, die evenredig is met de bekkenlengte.

Vervolgens is het model geanalyseerd door een ontwikkeling te maken in twee kleine parameters, namelijk ϵ en β . De eerstgenoemde geeft de verhouding van de verticale getij-amplitudo en de waterdiepte op de zeewaartse rand, de tweede de amplitudeverhouding van het M_4 - en M_2 -getij op de open rand. De overige belangrijke modelparameters zijn de fase van het M_4 -getij op de open rand, de bodemwrijvingscoëfficiënt en de lengte van het bekken. Vooralsnog is alleen gezocht naar morfodynamische evenwichten, die gekenmerkt worden door de afwezigheid van een netto sedimentflux in het gehele bekken. De oplossingen zijn berekend met behulp van continuatietechnieken, dat wil zeggen uitgaande van bekende oplossingen (in de korte bekkenlimiet) worden oplossingen geconstrueerd door bepaalde parameters (bekkenlengte, sterkte van het externe M_4 -getij, etc.) geleidelijk te veranderen.

Allereerst is de situatie onderzocht waarbij er geen extern opgelegde hogere harmonischen van het basisgetij werden beschouwd, d.w.z. parameter $\beta = 0$. De resultaten zijn weergegeven in figuur 4, voor een discussie van de parameters in deze figuur, zie secties 2 en 3. Alle overige parameters zijn zodanig gekozen dat ze representatief zijn voor de Westerschelde. Opvallende kenmerken zijn dat in het korte bekkenregime het bodemprofiel een nagenoeg constante helling heeft. Voor toenemende bekkenlengte wordt dit profiel steeds meer concaaf, als gevolg van traagheids- en continuïteitseffecten en de toenemende invloed van bodemwrijving. Als de bekkenlengte ongeveer een kwart is van de wrijvingsloze getijgolfengte treedt er resonantie op van het M_2 -getij. Voor nog grotere bekkenlengten ontstaat een bodemprofiel waarbij vanaf de zeewaartse rand de waterdieptes eerst toenemen en pas achterin sterk afnemen. Dit laatste hangt samen met de opwekking van een sterk M_4 -horizontaal getij achterin het bekken als gevolg van bodemwrijving. Teneinde de daarmee samenhangende netto transporten te neutraliseren krijgt de bodem achterin het bekken een convex profiel. De getijgolf verandert qua karakter steeds meer van een staande golf naar een lopend golf. Voor een bekkenlengte groter dan de wrijvingslengteschaal

van het bekken (zo'n 220 km, d.w.z. ongeveer 40% van de wrijvingsloze getijgolf lengte) bestaat er geen morfodynamisch evenwicht meer. De conclusies zijn dus dat ook lange bekkens morfodynamische evenwichten hebben en dat ze bij afwezigheid van externe overtides uniek zijn. Echter voor bekkenlengten groter dan de wrijvingslengteschaal van de getijgolf bestaan geen evenwichten meer.

Het toelaten van externe overtides in het model leidt tot wezenlijke nieuwe verschijnselen. Dit komt omdat naast het M_2 -getij ook het externe M_4 -getij resonantiegedrag vertoont. Vooralsnog is alleen het geval onderzocht waarbij het faseverschil tussen de twee getijcomponenten op de zeewaartse rand 0 graden is, zoals het geval is bij de Westerschelde. Voor relatief korte bekkenlengten zijn sedimentfluxen geïnduceerd door externe overtides veel groter dan degene die bepaald worden door intern gegenereerde overtides. Als gevolg hiervan hebben deze evenwichten significant andere kenmerken, zie figuur 7. De waterdiepten nemen vanaf de zeewaartse rand naar binnen sterk toe en bereiken een maximum ongeveer halverwege het bekken. De maximale waterdiepte wordt bereikt bij een bekkenlengte van ongeveer 110 km en bedraagt, in het geval van de Westerschelde, meer dan 60m. Dit evenwicht kan echter niet langer bestaan voor lengten groter dan 160km, hetgeen de wrijvingslengteschaal van het externe M_4 -getij is. De bijbehorende getijgolf blijkt vooral een staand karakter te hebben.

Interessant is dat er voor grotere bekkenlengten nog evenwichten kunnen bestaan, die qua eigenschappen sterk overeenkomen met de evenwichten die hiervoor zijn beschreven. Deze bestaan in het geval $\beta = 0.07$, hetgeen representatief is voor de Westerschelde, voor bekkenlengten tussen de 140 en 180km. De belangrijke constatering hierbij is dus dat het model het bestaan van meerdere evenwichten bij dezelfde parameterwaarden toestaat. Het eerste type evenwicht wordt bepaald door een balans tussen sedimentfluxen die geïnduceerd worden door extern geforceerde getijasymmetrie; het tweede type evenwicht is gerelateerd aan interne getij-asymmetrie. Voor afnemende waarden van β zijn deze evenwichten steeds minder van elkaar te onderscheiden en vloeien uiteindelijk samen. Het bestaan en verdwijnen van deze verschillende typen evenwichten kan worden begrepen vanuit fysische principes: bodemwrijving is bepalend voor het 'interne' evenwicht, de amplitude van het externe overtide voor het 'externe' evenwicht en het bestaan van meerdere evenwichten treedt alleen op als de kortste bekkenlengte, waarbij een 'intern' evenwicht kan bestaan, dicht in de buurt ligt van de resonantielengte van het extern gegenereerde overtide. Indien dit niet het geval is blijkt er een geleidelijke overgang te zijn van een 'extern' naar een 'intern' evenwicht.

Ter illustratie en test is het model ook gebruikt om de effecten van de constructie van de stormvloedkering op het morfologisch gedrag van het Oosterscheldebekken te berekenen. Dit resulteerde in een voorspelling dat de verandering in getijdebewegingen zodanig zijn dat er een zandtekort is in het bekken van ongeveer $250 \times 10^6 \text{ m}^3$. Dit is van dezelfde orde van grootte als het op waarnemingen geschatte zandtekort, hetgeen een bevestiging is van de potentiële kracht van geïdealiseerde modellen.

Het bestaan van meerdere evenwichten en de bijbehorende stabiliteitseige-

schappen kan belangrijke consequenties hebben voor het beheer van getijdebekkens. Teneinde dit te onderzoeken is een numeriek model geconstrueerd dat de tijdsontwikkeling van bodemprofielen, en de daaraan gekoppelde waterbeweging en sedimentfluxen, beschrijft. Dit model bevindt zich nog in de testfase, veroorzaakt door het feit dat de bodemverandering op de landwaartse rand bij lange bekkens niet nul is. Als gevolg hiervan is ook de lengte van het bekken een dynamische variabele, hetgeen een cruciaal verschil is met korte bekkens. Resultaten worden op korte termijn verwacht.

One-dimensional long-term equilibria of tidal embayments

H.M. Schuttelaars

27th February 2003

Abstract

A one-dimensional model for a long tidal embayment is developed and analyzed. It is a generalization of earlier work to domains in which vertical tide is spatially nonuniform such that bottom friction and inertial effects play an important role in the dynamics. The system is driven by a prescribed external M_2 and M_4 -tide. Furthermore overtides are generated internally. It is demonstrated that the model allows for morphologic equilibria characterized by an equilibrium bed profile that has a prescribed depth at its entrance and a zero water depth at the land-side of the embayment. For short embayments (length much shorter than the tidal wave length), the bed has approximately a constantly sloping profile and the velocity is spatially uniform. If the length is increased the bed becomes concave and the velocity becomes spatially non-uniform. If the system is only forced by an externally prescribed M_2 -tide and other parameter values representative for the Western Scheldt, no equilibrium profile can be found anymore for an embayment with a length larger than $0.45 L_g$ with $L_g = 2\pi\sqrt{gH}/\sigma$. The maximum embayment length depends, among others, on the frictional strength and the externally prescribed overtide. If an externally prescribed overtide is forcing the system as well, more than one type of equilibrium can be found. The two equilibria have totally different characteristics: for one of them advective fluxes due to internally generated and externally forced overtides make an approximate balance. The effect of bottom friction is small and the tidal motion has the characteristics of a standing wave. The bed can become very deep, up to 7 times the depth at the entrance of the embayment. The other equilibrium is frictionally modified and characterized by a balance between internally generated advective fluxes. The maximal bed depth is of the order of twice the depth at the entrance and a travelling wave character is observed. The first type of equilibrium exists for lengths $(0, L_{MAX,1})$, the second one for $(L_{MIN,2}, L_{MAX,2})$. For certain values of the parameters, these two equilibria can coexist. Hence multiple equilibria can exist. Furthermore, the maximum embayment length becomes shorter when the ratio of the amplitudes of the M_4 - and M_2 -tides ($\equiv \beta$) is increased. If $\beta = 0.074$ the first equilibrium exists up to $L_{MAX,1} = 0.28L_g$ and the second one exists in the interval $(0.26L_g, 0.33L_g)$.

1 Introduction

The morphology of many tidal inlets and estuaries is characterized by a complex pattern of channels and sandy shoals, both in space and time. This dynamic behaviour is caused by the feedback between the water motion, sediment transport and bottom changes. Observations clearly indicate that morphological behaviour is sensitive to changes in external conditions caused e.g. by sealevel rise and/or human interferences (Van der Spek, 1997). Both for economical and ecological reasons there is a strong need to simulate and predict both the morphological processes and the sensitivity of the morphology on changing conditions.

Figure 1: The marine salt and brackish part of the Western Scheldt estuary from Vlissingen to Antwerp.

In this report the emphasis is on the Western Scheldt, an estuary located in the the south-west of Holland and Belgium (see figure 1), which serves as the main navigation lane to the harbour of Antwerp. In the Western Scheldt economical and ecological interests often interfere. For shipping purposes it would be advantageous if the channel was canalized. On the other hand, the Western Scheldt has important feeding grounds for birds and other animals for which the system has to be kept as dynamic as possible. To keep the harbour open for large ships, the navigation lane of the Western Scheldt has to be dredged continuously ($8 \cdot 10^6 \text{ m}^3 \text{ year}^{-1}$) (Verbeek *et al.*, 1998).

The estuary has a length of approximately 160 kilometers with a marine

part of 60 kilometers. The depth at the mouth near Vlissingen is varies from 10 to 25 meters, it reaches a maximum near Terneuzen, 15 kilometers upstream of Vlissingen, of about 50 meters after which the depth decreases again. The water motions are driven at the sea side by an M_2 -tide with amplitude 2.0 m and an M_4 -overtide with amplitude 0.13 m. The phase difference between the M_2 and M_4 -tide is nearly 0° at the entrance and increases to 180° near Antwerp. The average river discharge is $110 \text{ m}^3\text{s}^{-1}$, which is less than one percent of the tidal water fluxes at the Dutch–Belgium boundary. Hence the system is well-mixed (?).

The sediment consists of fine sand with an average grain size of 0.2 mm and is mainly transported as suspended load. The number of main channels decreases from three at the mouth of the estuary to one at its end. The ebb channels meander on a scale of about 5 km, whereas the flood channels are straight. The secondary channels show a much more complex behaviour. Connecting channels as described in Jeuken (1998) exhibit cyclic behaviour. Furthermore, fractal bottom patterns can be found in parts of the estuary, such as the "Verdronken Land van Saaftinge".

In recent years there have been substantial developments regarding the simulation of morphological processes in the Western Scheldt with the use of models based on first principles (?De Jong, 1998)). However, due to lack of process knowledge, such models are as yet not suitable to simulate the long-term evolution of channel–shoal patterns. This motivates the simultaneous use of idealized models since they capture the essential physics but can still be analyzed using mathematical methods. In Schuttelaars (1997) it was shown that with this approach periodic behaviour and the splitting of channels that resembles behaviour as observed in short embayments (i.e. the embayment length is short compared to the tidal wave length), could be simulated. The important issue is to generalize this method to longer embayments, such as the Western Scheldt, which are considerably more complicated to analyze due to the influence of inertia and friction on the water motions (see ?).

In this paper the analysis will be restricted to a one-dimensional model, since this provides the information necessary to perform a two-dimensional analysis resulting in channel–shoal behaviour. The main questions that will be addressed are

- Do equilibria exist in long embayments?
- What are the underlying important physical processes?
- What is the sensitivity of these equilibria for changes in parameters?

Important generalizations with respect to Schuttelaars & De Swart (1996) are the spatial variations of both the vertical and horizontal tide. Furthermore, in a long channel the net transport of suspended sediment will be mainly due to advection, whereas in a short embayment the main transport mechanism is diffusive transport (see section 5). Important differences with De Jong (1998) are the negligence of river influence and the incorporation of diffusive boundary layers in the averaged concentration equation.

In section 2 the model will be presented, in section 3 the equations are scaled and analyzed using an asymptotic method. In section 4 the short embayment regime is studied. In section 5 the existence of equilibria and an explanation for the observed characteristics of the equilibrium bedforms is given. In the last section some conclusions and suggestions for future work will be made.

2 Model Description

The embayment under study is a rectangular basin. If for a short embayment one assumes the waterdepth to become zero at the landward end, the equilibrium bed profiles obtained are such that a spatially uniform shear stress distribution is attained, which seems to be consistent with field observations (Friedrichs, 1995). Moreover, the relation between cross-sectional area and the tidal prism appears to be linear as data indicate (De Vriend, 1996). Therefore it is assumed that in case of a long embayment the influence of the river inflow is not present or can be neglected (as is the case in the Western Scheldt, since the river inflow is only one percent of the tidal water fluxes at the Dutch–Belgium border). This assumption leads to an embayment that has a zero water depth at the landward end. The width is much smaller than both the length of the embayment and the Rossby deformation radius, which permits to model the embayment as one-dimensional (no variations in the cross-channel direction). The system is forced with an externally prescribed vertical tidal elevation ζ with respect to the undisturbed water depth at the entrance. Note that due to surface elevations the boundary at the end of the embayment is a *moving* boundary (see figure 2, where the length, corresponding to sea level ζ_1 and ζ_2 is denoted by L_1 and L_2 , respectively). The

Figure 2: Cross-sectional view of the embayment.

reference water depth is denoted by H , the bed elevation by h and u denotes the horizontal tide.

The water motions are described by the depth-averaged shallow water equations for a homogeneous fluid (Csanady, 1982):

$$\zeta_t + [(H - h + \zeta)u]_x = 0 \quad (1a)$$

$$u_t + uu_x + g\zeta_x + \hat{r} \frac{u}{H - h + \zeta} = 0 \quad (1b)$$

with $\hat{r} = 8UC_D/3\pi$, where U is a characteristic velocity scale and $C_D \sim 0.002$ the drag coefficient. The bottom friction in the momentum equation (1b) is

linearized (see Lorentz (1922); Zimmerman (1982, 1992)). At the open boundary the tidal elevation ζ is prescribed. At the closed end, the kinematic boundary condition is used. This condition requires u_x to be finite (see appendix C).

The sediment in the embayment consists of noncohesive material with only one grain size and is mainly transported as suspended load. This transport is described by a depth-integrated concentration equation (see Van Rijn (1993)):

$$[C_t + (uC - \mu_* C_x)_x] = \alpha u^2 - \gamma C \quad (2)$$

Here C is the depth-integrated sediment concentration, *i.e.*, the amount of sediment stored in a column sea water with unit horizontal area and μ_* is a constant diffusion coefficient of order $100 \text{ m}^2 \text{ s}^{-1}$. The sedimentation at the top of the active layer consists of the whirling up and settling of sediment. The sediment pick-up function is parametrized as αu^2 , where α is a coefficient related to sediment properties (grain size, shape, etc.). This parameterization is motivated by the analysis of field observations reported by Dyer & Soulsby (1988), see also Fredsoe & Deigaard (1992). Typical values of α are $\mathcal{O}(10^{-2} - 10^{-4} \text{ kgsm}^{-4})$ corresponding to fine and medium sand, respectively.

The term $-\gamma C$ models the deposition of the sediment. The constant γ can be related to the settling velocity and a diffusion coefficient κ_v that describes the mixing of the sediment in the vertical. Assuming a constant κ_v it follows from Van Rijn (1993) that $\gamma = w_s^2 / \kappa_v$ with characteristic values of $4 \cdot 10^{-3} \text{ s}^{-1}$. The boundary condition for the concentration equation is that the sediment flux at the moving boundary is zero. In appendix C this is discussed in more detail. At the entrance it is imposed that the bed does not change. Since the bed only changes due to tidally averaged erosion and deposition, additional boundary conditions are needed. We therefore require that no diffusive boundary layer develops at the entrance of the embayment in the time-varying concentration. Thus near $x = 0$ the solution for C in the limit $\mu_* \rightarrow 0$ should be consistent with the solution of the concentration equation (2) with $\mu_* = 0$.

The bottom evolution equation can be derived from continuity of mass in the sediment layer and reads

$$\rho_s(1-p)h_t = -\langle \alpha u^2 - \gamma C \rangle = -F_x \quad (3)$$

with p (~ 0.4) the bed porosity and ρ_s ($\sim 2650 \text{ kgm}^{-3}$) the density of the individual grain particles. Note that for the bed evolution equation (3) no boundary conditions are required, only an initial condition must be supplied. Since at $x = 0$ the total deposition equals the erosion, the bed remains fixed at $x = 0$, at the end the water depth is always zero.

3 Scaling and Expansion

The equations as proposed in section 2 are scaled using

$$\begin{aligned} x &= L\tilde{x}, t = \tilde{t}\sigma^{-1}, u = \frac{A\sigma L}{H}\tilde{u} \\ \zeta &= A\tilde{\zeta}, h = H\tilde{h}, C = \frac{\alpha U^2}{\gamma}\tilde{C} \end{aligned} \quad (4)$$

Here L is chosen such that $x = 1$ is the intersection point of the bed profile and the undisturbed water level. The radian frequency of the main tidal constituent is denoted by σ and A is the amplitude of the vertical tide at the entrance. Suppressing the tilde, the equations read

$$\zeta_t + [(1 - h + \epsilon\zeta)u]_x = 0 \quad (5a)$$

$$u_t + \epsilon uu_x + \lambda_L^{-2}\zeta_x + r\frac{u}{1 - \alpha(h - \epsilon\zeta)} = 0 \quad (5b)$$

$$a[C_t + (\epsilon uC - \mu C_x)_x] = u^2 - C \quad (5c)$$

$$h_\tau = -\langle u^2 - C \rangle \quad (5d)$$

Here ϵ is, apart from a factor of 2π , the ratio of the tidal excursion (the distance travelled by a fluid particle in a tidal period) and the tidal inlet length (for the definitions of the nondimensional parameters in the model, see table 1). The constant λ_L is the ratio of the frictionless tidal wave length L_g and the

Parameters in the nondimensional model

$$\begin{aligned} \epsilon &= \frac{A}{H} = \frac{U}{\sigma L} & \lambda_L &= \frac{2\pi L}{L_g} & r &= 8C_D AL / (3\pi H^2) \\ a &= \frac{\sigma}{\gamma} & \mu &= \frac{\mu_s}{\sigma L^2} & \delta_s &= \frac{\alpha U^2}{\rho_s(1-p)H\sigma} \end{aligned}$$

Table 1: Parameter definitions in the nondimensional model.

embayment length, and r is a measure for the frictional strength. The parameter α in the bottom friction is used to vary the influence of the depth on the friction; since $1 - h + \epsilon\zeta$ becomes zero at the end of the embayment, this term would become infinite, which is not a very realistic parameterisation of the bed friction. Since the friction becomes large but finite when the water depth becomes small, α is chosen to be close to 1.

Furthermore, a is the ratio of the timescale of the deposition process and the tidal period and μ is the ratio of the tidal period and the diffusive time scale. Here $\tau = \delta_s t$ is a long time scale.

The boundary conditions at the entrance $x = 0$ are

$$\zeta = \cos(t) + \beta \cos(2t - \phi) \quad (6a)$$

$$h = 0 \quad (6b)$$

$$C(x, t, \mu) = C(x, t, \mu = 0) \quad (6c)$$

Here β is the ratio of the M_4 amplitude and the M_2 amplitude at the entrance, ϕ is the phase difference between the M_4 and M_2 tidal constituents at this location, defined by $\phi = \phi_{M_4} - 2\phi_{M_2}$. At the closed end the boundary conditions read (see appendix C.2)

$$u_x \text{ is finite} \quad (7a)$$

$$\langle \epsilon u C - \mu C_x \rangle = 0 \quad (7b)$$

$$C'(x, t, \mu) = C'(x, t, \mu = 0) \quad (7c)$$

where C' is the oscillatory part of the concentration equation. The first boundary condition is the kinematic boundary condition, the second one states that no net sediment flux is allowed through $x = 1$. The boundary condition for the time-varying concentration states that no diffusive boundary layer is found at the end of the embayment in the oscillatory fluxes. This is discussed in more detail in section C.

These equations will be solved by making an expansion with respect to the small parameters ϵ and β , up to first order. No assumption on the ratio of ϵ and β is made. It is only assumed that $\beta \ll 1$, *i.e.* that the M_2 constituent is much stronger than the externally prescribed M_4 constituent. Hence for the water elevation ζ the following expansion is made

$$\zeta = \zeta_0 + \epsilon \zeta_1 + \beta \zeta_{o,1} \dots \quad (8)$$

with

$$\begin{aligned} \zeta_0 &= \zeta^s \sin(t) + \zeta^c \cos(t) & \zeta_1 &= \zeta^0 + \zeta^{2s} \sin(2t) + \zeta^{2c} \cos(2t) \\ \zeta_{o,1} &= \zeta_o^{2s} \sin(2t) + \zeta_o^{2c} \cos(2t) \end{aligned}$$

Here ζ_0 describes the main tidal constituent and ζ^0 the mean water level which is induced by net transfer of momentum by the tidal wave. Furthermore ζ^{2c}, ζ^{2s} are the internally generated M_4 -overtide and $\zeta_o^{2s}, \zeta_o^{2c}$ the M_4 -overtide generated by external forcing. Similar expansions for u and C can be made. The same notation is used as in the above expansion (use of superscripts to describe the temporal behaviour on the short time scale and the subscripts to make a distinction between internally generated and externally driven quantities). Of course, one can write $\zeta_0 = |\zeta_0| \cos(t - \phi_{\zeta_0})$, etc., as well. Here $|\zeta_0|$ is the amplitude of the M_2 vertical tidal elevation, ϕ_{ζ_0} its phase angle.

If a bed profile and the surface elevations at the entrance of the embayment are given, the horizontal and vertical velocities and the concentration can be calculated explicitly. This information is used to calculate a net sediment flux F and to rewrite the bed evolution equation as

$$h_\tau = -F_x(h, h_x, h_{xx}) \quad (9)$$

Hence the bed changes due to divergences or convergences of the sediment flux. From (9) it is clear that an equilibrium bed profile is found if $h_\tau = 0$. Using

the boundary conditions on the sediment flux (7b), this means that in equilibrium the net sediment flux throughout the embayment has to be zero. After expanding the flux in the small parameter ϵ , this condition reads

$$F = -a\mu C_x^0 + a\epsilon^2 \left(u^0 C^0 + \frac{1}{2} [u^s C^{s} + u^c C^c + u^{2s} C^{2s} + u^{2c} C^{2c}] \right) + a\frac{1}{2}\epsilon\beta (u^s C_o^s + u^c C_o^c + u_o^{2s} C^{2s} + u_o^{2c} C^{2c}) = 0 \quad (10)$$

So if an equilibrium bed profile is found, the combination of the velocity and concentration fields as given in (10) is such that the total time-averaged flux is zero. Using the knowledge of the equilibrium solution in case of the short embayment limit (see Schuttelaars & De Swart (1996)) and standard numerical methods (continuation techniques in slowly varying parameters), equilibrium bed profiles and their corresponding velocity fields, surface elevations and concentration fields for different embayment lengths, tidal forcing etc. can be obtained.

4 The Short Embayment Regime

In this section, the results obtained by Schuttelaars & De Swart (1996) in the limit $\lambda_L \equiv L/L_g \rightarrow 0$, *i.e.*, a short embayment, will be compared with the results obtained when small but finite values of λ_L are considered. The parameters used are given in table 2.

Quantities in the dimensional model

$$\begin{array}{lll} H \sim 10 \text{ m} & L \sim 2 \cdot 10^4 \text{ m} & \sigma \sim 1.4 \cdot 10^{-4} \text{ s}^{-1} \\ A \sim 1.5 \text{ m} & \mu_* \sim 10^2 \text{ m}^2 \text{ s}^{-1} & C_D \sim 1 \cdot 10^{-3} \end{array}$$

Parameters in the nondimensional model

$$\begin{array}{lll} \epsilon \sim 0.15 & a \sim 0.04 & \mu \sim 1.8 \cdot 10^{-3} \\ \delta_s \sim 8 \cdot 10^{-4} & \lambda_L^2 \sim 0.078 & r \sim 1.7 \\ \beta \sim 0.5 & \phi \sim 7^\circ & \end{array}$$

Table 2: Quantities and parameter values for the Frisian inlet system.

In Schuttelaars & De Swart (1996) the correction terms of order λ_L^{-2} in (5b) were neglected. It was found that if the forcing does not contain overtides the suspended load model has a unique stable equilibrium which represents a constantly sloping bottom with zero depth at the closed end and spatially uniform tidal currents.

In the complete model, the influence of the order λ_L^{-2} terms is taken into account. If the sediment is only transported due to diffusion, C_x has to be zero, which implies that to a good approximation the velocity amplitude is constant (the relative error is at most of order ϵ , which is much smaller than 1). However, the bed profile is not exactly a constantly sloping bottom. This can

be understood as follows: neglect terms of order ϵ in the equations of motion, and expand u and ζ in the small parameter λ_L^{-2} . The velocity fields become

$$u^s = - (1 + \lambda_L^2 x + \dots) \sin(t)$$

and u^c is of order λ_L^2 . Hence $\langle u^2 \rangle \sim 1 + 2\lambda_L^2 x + \mathcal{O}(\lambda_L^4)$ increases towards the end of the embayment due to resonance effects. Furthermore, to compensate for bottom friction the pressure gradients increase towards the end of the embayment and hence $|u|$ increase even more. Since the time averaged concentration is in first order proportional to $\langle u^2 \rangle$, the concentration increases as well. Due to diffusive processes, sediment has to be moved out of the estuary and the initial bed profile has to become concave.

Since for a short embayment advective processes behave as diffusive ones (Schuttelaars & De Swart, 1996), introduction of advective transport results in a concave bed profile as well (see figure 3).

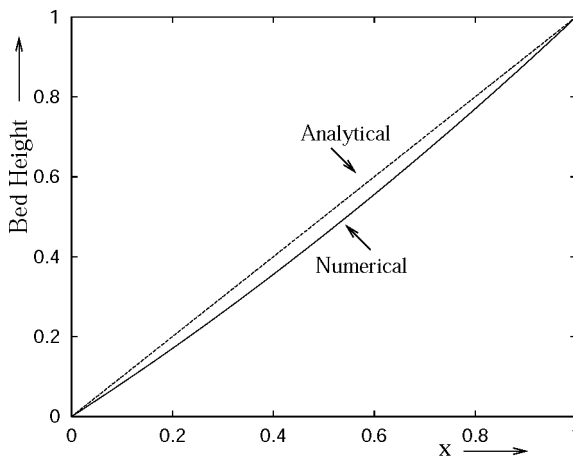


Figure 3: Analytical (no λ_L^2 corrections) and numerical equilibrium bed profiles are plotted for an embayment with length $L = 2 \cdot 10^4$ m. The parameters used are given in table 2.

The introduction of overtides in the forcing resulted in more complex dynamics. The equilibrium bottom profiles in the suspended load model could become convex or concave, depending on the ratio of advective and diffusive transports. This behaviour is reproduced by the numerical model as well, for $\phi < 0$ concave bottom profiles are found, for $\phi > 0$ convex ones are obtained.

5 Numerical Experiments

In the numerical experiments, the influence of different parameter values on the maximum embayment length and the number of possible morphodynamic equilibria is investigated. One of the most interesting questions is whether an equili-

Quantities in the model

$$\begin{array}{lll}
 H = 15 \text{ m} & A = 1.0 \text{ m} & \sigma \sim 1.4 \cdot 10^{-4} \text{ s}^{-1} \\
 \mu_* = 10^2 \text{ m}^2 \text{ s}^{-1} & a = 0.01 & C_D = 1 \cdot 10^{-3} \\
 \beta \sim 0.074 & \phi \sim 1^\circ &
 \end{array}$$

Table 3: Quantities and parameter values used in the numerical experiments with variable embayment length. They are representative for the Western Scheldt

Equilibrium exists for all embayment lengths for a given set of parameters. Therefore, usually the length will be varied for some parameter values. The default values used in the experiments are given in table 3 and are based on parameters obtained from observations in the Western Scheldt estuary (see De Jong (1998)).

5.1 No Overtides

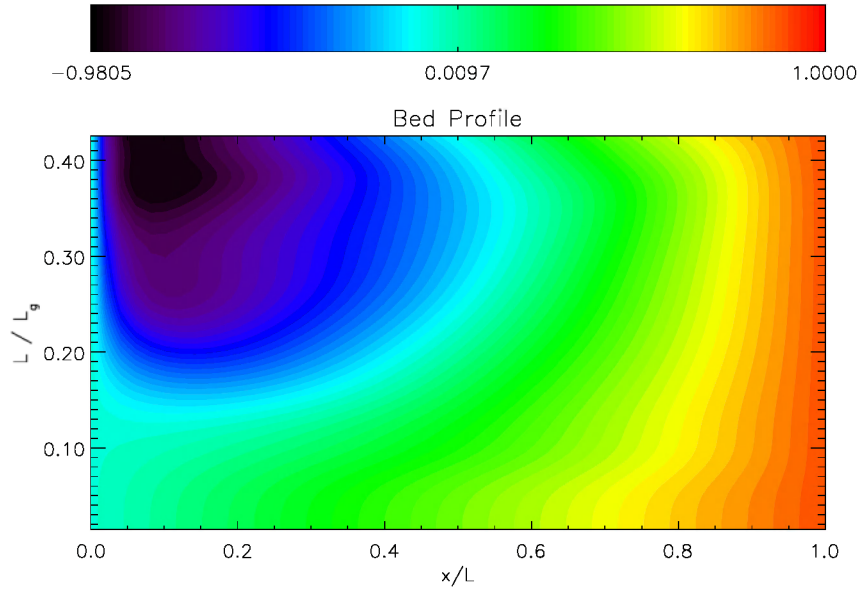


Figure 4: Contour plot of the equilibrium bed profile for different embayment lengths as a function of x/L . Here $L_g \sim 550$ km. The system is only forced with an externally prescribed M_2 -tide.

In this experiment the embayment length varies under the assumption that

the system is only driven by an externally prescribed M_2 -constituent, higher constituents are only generated internally by nonlinear interactions. Thus $\beta = 0$ in this experiment. In this experiment the embayment length is varied. The other parameters are as given in tabel 3. Note that due to variation of the embayment length the scaled diffusion constant $\mu = \mu_*/\sigma L^2$, the friction coefficient r and the ratio of the tidal period and the morphological time-scale δ_s change. This means that the relative importance of advective sediment fluxes (which scale with ϵ^2) over diffusive fluxes become more important.

From figure 4 it can be seen that the equilibrium bed profile is a straight line for small L , if L is increased the bed becomes deeper near the entrance of the embayment. This phenomenon was already explained in the case of a short embayment (see section 4). A maximum depth of about 27 m is reached near $L = 210$ km. For $L \gtrsim L_{\text{MAX}}$, with $L_{\text{MAX}} \sim 240$ km, slightly less than half the frictionless tidal wave length, no equilibrium bed profile can be found anymore: if one starts with a embayment length \tilde{L} larger than 240 km, the undisturbed water becomes zero near $x = L_{\text{MAX}}/\tilde{L}$. So effectively the embayment length is again L_{MAX} . The maximum embayment length equals the frictional length for the M_2 -tide, defined by $L_f^{M_2} = 8C_D L/3\pi H$.

In figure 5(a) and 5(c), the amplitude of the equilibrium horizontal tide is plotted. Note that M_2 tide becomes resonant for an embayment length of approximately 140 km. This is agreement with the well-known quarter-wave resonance of a frictionless tidal wave. This is quite surprising since the effects of bottom friction and the bottom profile strongly influence the resonance length. It appears that, if bottom friction is taken into account, the bottom profile in the estuary is changed in such a way that the embayment becomes resonant for $L = 0.25L_g$.

From figures 5(b) and 5(d) it is clear that the character of the tidal wave changes with increasing length: for $L \ll L_g$, a standing wave is observed in the embayment, if L increases the characteristics of a travelling wave are observed.

In the figures of the sediment fluxes, it is seen that diffusion is only important in a thin boundary layer at the entrance of the embayment (see figure 6(a)) for $L/L_g > 0.2$ and at the end of the embayment for $L/L_g > 0.3$. Furthermore, in a region with $L/L_g \ll 1$, where the transport is diffusively dominated. However, this cannot be seen from the figures because in equilibrium the diffusive flux has to be zero throughout the embayment. For larger embayment lengths, it is seen from figures 6(a)–6(f) that the fluxes due to interaction of externally forced M_2 velocities and internally generated concentrations balance and those due to internally generated horizontal concentrations and externally forced M_2 velocities. Since for these kind of equilibria the internal generation of phase differences in the velocity and concentration fields due to bottom friction are essential, this kind of equilibria will be called *frictionally modified equilibria*.

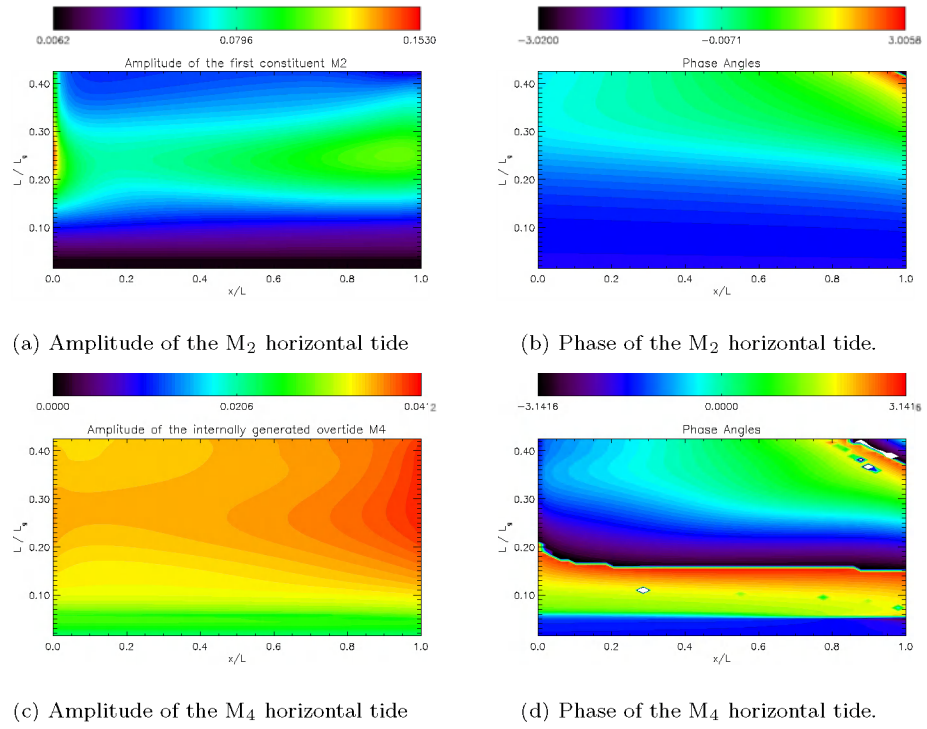


Figure 5: Contour plots of the amplitude and phase of the M_2 and M_4 horizontal tide as a function of embayment L/L_g and x/L . The velocities are scaled with the characteristic velocity \sqrt{gH} .

(a) Net diffusive sediment flux.

(b) Net sediment flux due to the advective contribution $u^0 C^0$.

(c) Net sediment flux due to the advective contribution $u^s C^{2s}$.

(d) Net sediment flux due to the advective contribution $u^c C^c$.

(e) Net sediment flux due to the advective contribution $u^{2s} C^{2s}$.

(f) Net sediment flux due to the advective contribution $u^{2c} C^{2c}$.

Figure 6: Contour plots of the leading order sediment fluxes as function of the scaled embayment length L/L_g and x/L . Here $L_g = 2\pi\sqrt{gH}/\sigma \sim 550$ km and $\beta = 0.0$ for the equilibrium bed profile as shown in figure 4. The amplitudes of the fluxes are scaled with $(\alpha/\gamma) (\epsilon\sqrt{gH})^3$.

5.2 Overtides, no phase difference

In this subsection an externally prescribed overtide is introduced with a phase difference $\phi = 0^\circ$. The ratio of the M_4 amplitude and the M_2 amplitude, β is chosen to be 0.05. The other parameters were unchanged.

The most remarkable change from the situation with no overtide is that, instead of one unique equilibrium, two equilibria for the same parameter values can be found if the strength of the overtide is increased. These two bed equilibria differ considerable from each other. One of the equilibria becomes very deep, up to 60 m, while the other equilibrium is much shallower.

In case of a short embayment ($L/L_g \ll 1$) it was shown in Schuttelaars & De Swart (1996) that if sediment was transported due to externally prescribed M_2 - and M_4 -forcing, only one equilibrium could exist. From the results obtained with the model described in section 2, it turns out that this is still the case if advective transport due to both internally generated and externally prescribed M_4 is taken into account. If the length is increased and the externally prescribed overtide is strong enough, multiple equilibria can be found. It appears that, if the different contributions to the sediment flux equation (10) are studied in more detail, one of these equilibria (the deep equilibrium) is characterized by large fluxes due to the interaction of the external overtide with the basic tide are balanced by interactions of internally generated overtides with the basic tide. In this equilibrium frictional effects are very small. The other equilibrium is frictionally dominated. In this shallow equilibrium sediment fluxes due to the external forcing are one order smaller than the fluxes due to internally generated overtides.

If the parameter $\beta = 0.05$, the external forcing is not strong enough to result in multiple equilibria. Hence only one equilibrium profile is found (see figure 7). However, it changes its character dramatically just after resonance. Using figures 8(a), 8(c) and 8(e), it can be seen that the M_2 -tide becomes resonant for an embayment length of $L \sim 0.25L_g$, whereas the externally forced M_4 tide becomes resonant for lengths of approximately $0.18L_g$. Note that the resonance of the M_4 -tide is consistent with the resonance length of the M_2 -tide:

$$L_{\text{Res}}^{M_4} = \frac{1}{4}L_g^{M_4} = \frac{\sqrt{2}}{4}L_g^{M_2}$$

with $L_{\text{Res}}^{M_4}$ the resonance length of the M_4 -tide, $L_g^{M_2}$ and $L_g^{M_4}$ the frictionless tidal wave length of M_2 and M_4 respectively.

If $L \ll L_g$, the equilibrium is diffusively dominated. If L is increased but smaller than the M_4 frictional length $L_f^{M_4}$, equilibria that is characterized by large water depth (approximately 3 times the depth at the entrance), are found. The maximum depth is reached for a length of approximately $0.25L$. The water motions have the characteristics of a standing wave (see figures 8(b), 8(d) and 8(f)). Frictional effects are negligible. An approximate balance between advective fluxes due to internally generated overtide contributions and those due to externally generated contributions is observed: the $\langle u^s C^s \rangle$ internally generated advective flux is balanced by $\langle u^s C_o^s \rangle$ (see figures 9(a) and 9(b)), the

flux due to $\langle u^{2c}C^{2c} \rangle$ is balanced by $\langle u_o^{2c}C^{2c} \rangle$ (see figures 9(c) and 9(d)), etc. Therefore, this equilibrium will be called *external equilibrium*.

If the length L is increased more ($L/LG > 0.2$), frictional effects become important and the other equilibrium is found: the bottom becomes less deep and the horizontal tide has a travelling wave character (see figures 8(b), 8(d) and 8(f)). The fluxes due to externally prescribed overtides decrease dramatically and a completely new balance is found: the $\langle u^s C^s \rangle$ internally generated advective flux is balanced by $\langle u^c C^c \rangle$ (see figures 9(a) and 9(e)), the flux due to $\langle u^{2c}C^{2c} \rangle$ is balanced by $\langle u^{2s}C^{2s} \rangle$ (see figures 9(c) and 9(f)), etc. This kind of equilibrium will be called *frictionally modified equilibrium*.

For the ratio of the M_4 - and M_2 -tide used above ($\beta = 0.05$), the shortest wave-length for which a frictionally modified equilibrium can exist and the resonance length of the M_4 -tide differ considerably. Hence a gradual change from the external equilibrium towards the frictionally dominated one is observed. If the resonance length of the M_4 -tide and the shortest possible frictionally dominated equilibrium are close together, multiple equilibria can exist. This means that for a fixed length of the embayment more than one equilibrium can exist! This is for example the case in the Western Scheldt with $\beta = 0.074$.

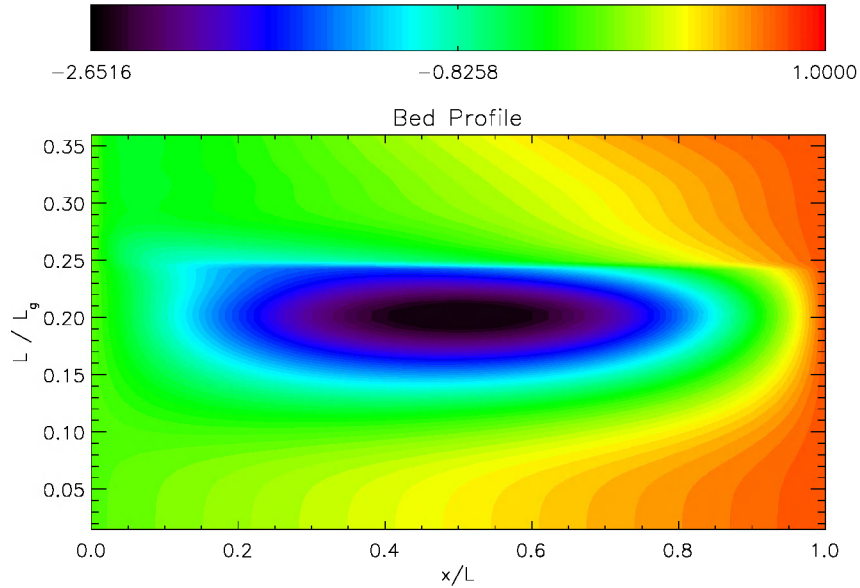
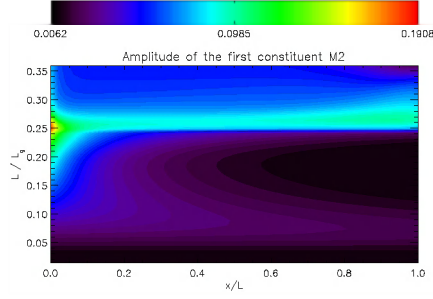
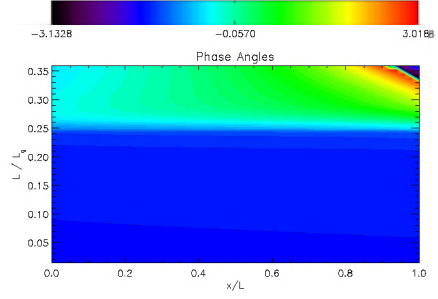


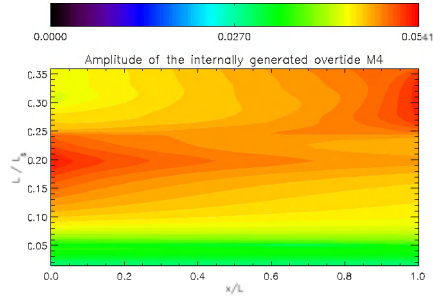
Figure 7: Contour plot of the equilibrium bed profile as function of the scaled embayment length L/L_g and x/L . Here $L_g = 2\pi\sqrt{gH}/\sigma \sim 550$ km, $\beta = 0.05$ and $\phi = 0^\circ$. The depth at the entrance of the embayment is 15 m.



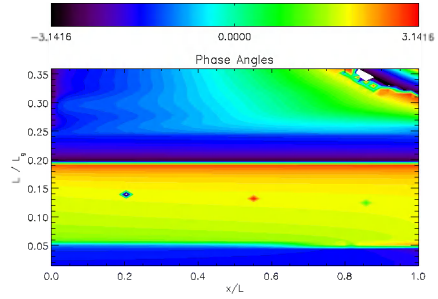
(a) Amplitude of the M_2 horizontal tide, associated to the bed profile in figure 7.



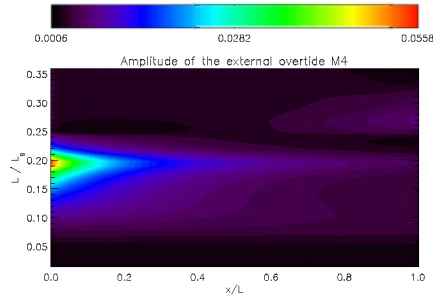
(b) Phase of the M_2 horizontal tide, associated to the bed profile in figure 7.



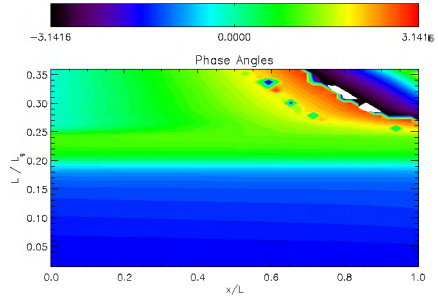
(c) Amplitude of the M_4 internally generated horizontal tide, associated to the bed profile in figure 7.



(d) Phase of the M_4 internally generated horizontal tide, associated to the bed profile in figure 7.

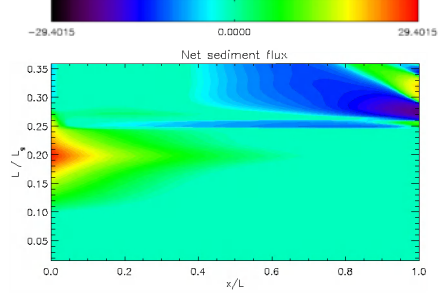


(e) Amplitude of the M_4 externally prescribed horizontal tide, associated to the bed profile in figure 7.

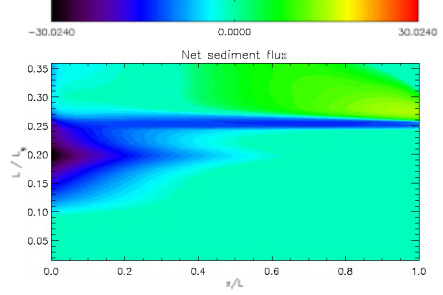


(f) Phase of the M_4 externally prescribed horizontal tide, associated to the bed profile in figure 7.

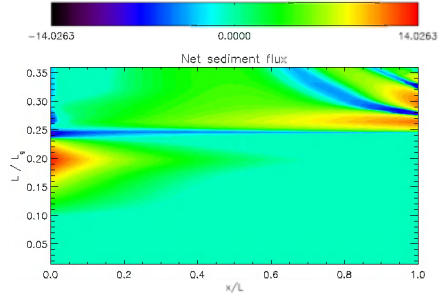
Figure 8: Contour plots of the amplitude and phase of the M_2 , internally generated and externally prescribed M_4 horizontal velocity profile as function of the scaled embayment length L/L_g and x/L . Here $L_g = 2\pi\sqrt{gH}/\sigma \sim 550$ km, $\beta = 0.05$ and $\phi = 0^\circ$. The amplitudes of the velocity are scaled with \sqrt{gH} .



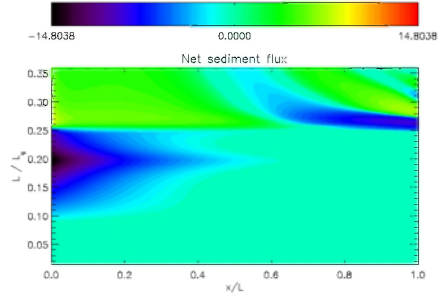
(a) Net sediment flux due to the advective contribution $u^s C^s$.



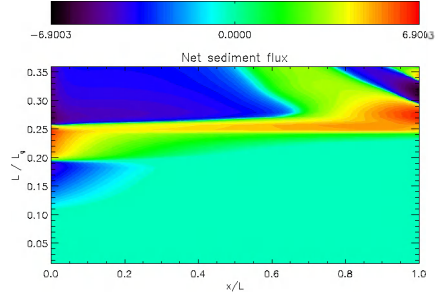
(b) Net sediment flux due to the advective contribution $u^s C_o^s$.



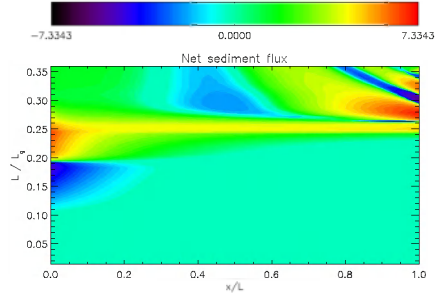
(c) Net sediment flux due to the advective contribution $u^{2c} C^{2c}$.



(d) Net sediment flux due to the advective contribution $u_o^{2c} C^{2c}$.



(e) Net sediment flux due to the advective contribution $u^c C^c$.



(f) Net sediment flux due to the advective contribution $u^{2s} C^{2s}$.

Figure 9: Contour plots of the leading order sediment fluxes as function of the scaled embayment length L/L_g and x/L . Here $L_g = 2\pi\sqrt{gH}/\sigma \sim 550$ km, $\beta = 0.05$ and $\phi = 0^\circ$ for the equilibrium bed profile as shown in figure 7. The amplitudes of the fluxes are scaled with $(\alpha/\gamma) (\epsilon\sqrt{gH})^3$.

6 Conclusions

In this report an idealized one-dimensional model is analyzed to gain more understanding of the morphodynamics in long embayments. The main aim in this report is to investigate the possible existence of equilibria. If the embayment length is much smaller than the tidal wavelength, the momentum equation describes in leading order a pumping mode, if the length is increased, both resonance effects and bottom friction become more important.

Sediment can be transported by diffusive and advective processes. For a short embayment, the diffusive transport mechanism is most important. However, if the channel length is increased, diffusion becomes less effective and advection is the main transport mechanism.

A system is said to be in morphodynamic equilibrium when the averaged sediment flux vanishes throughout the embayment. The water motions in the embayment are forced by both an externally prescribed M_2 - and M_4 -tide. Furthermore, overtides are generated internally. Using the knowledge of the short embayment limit and numerical continuation techniques, it is shown that equilibrium profiles exist for embayment lengths smaller than $L = L_{\text{MAX}} \sim L_f^{M_2} = 240$ km. Embayments longer than L_{MAX} tend to fill up until the maximum embayment length is reached. Of course, the maximum embayment length depends on external parameters, such as the depth at the entrance and the drag coefficient. The M_2 -tide becomes resonant for a length of approximately 0.25 times the gravitational wave length ($= 2\pi\sqrt{gH}/\sigma$), the M_4 -tide for approximately $\sqrt{2}/8L_g$.

Two types of equilibria are observed. One exists for $L < L_f^{M_4}$ and is called the external equilibrium: external M_4 -tides generate large sediment fluxes that are balanced by internally generated overtide contributions. Frictional effects are not important and the tides in the embayment have a standing wave character. The bed can become very deep and reaches its maximum halfway the embayment. The other equilibrium is much shallower and frictional effects are very important. The amplitudes of the external overtides are much smaller than those generated internally. This equilibrium is called the frictionally modified equilibrium. The water motions have a travelling wave character. This equilibrium exists for a certain range of embayment lengths. If the shortest wave-length for which a frictionally modified equilibrium can exist and the resonance length of the M_4 -tide differ considerably, a gradual change from the external equilibrium towards the frictionally dominated one is observed. If the resonance length of the M_4 -tide and the shortest possible frictionally dominated equilibrium are close together, more than one equilibrium can be found for one embayment length. This is for example the case in the Western Scheldt with $\beta = 0.074$.

As an illustrative example, the model has been used to investigate the possible sand deficit in the Eastern Scheldt (see appendix D) due to its partial closure. It was found that, to reach a new equilibrium, the embayment has to import $250 \times 10^6 \text{ m}^3$ sediment. This is the same order as magnitude as the predicted sand deficit.

A Dependence of resonance length on bed profile and frictional strength

In this appendix, we will study the effect of the bed profile and the frictional strength on the resonance length of the embayment. It is well known that a semi-enclosed embayment with a flat bed has its principal resonance if its length L equals 1/4 of the tidal wave length $2\pi\sqrt{gH}/\sigma$. If friction is introduced, the amplitude of the water excursion stay finite and the resonance length becomes shorter. However, most embayments do not have a flat bottom. Therefore it of importance to investigate the influence of a non-flat, but fixed, bottom on the resonance length L_{Res} .

Consider the following system of equations:

$$\zeta_t + [(H - h + \zeta)u]_x = 0 \quad (11a)$$

$$u_t + uu_x + g\zeta_x + \hat{r}\frac{u}{H - h + \zeta} = 0 \quad (11b)$$

with $\hat{r} = UC_D$, where U is a characteristic velocity scale and C_D the drag coefficient.

After making the equations dimensionless, using

$$\begin{aligned} x &= Lx^*, t = t^*\sigma^{-1}, u = \frac{a\sigma L}{H}u^* \\ \zeta &= A\zeta^*, h = Hh^* \end{aligned} \quad (12)$$

and suppressing the asterix, they read

$$\zeta_t + [(1 - h + \epsilon\zeta)u]_x = 0 \quad (13a)$$

$$u_t + \epsilon uu_x + \lambda_L^{-2}\zeta_x + r\frac{u}{1 - h + \epsilon\zeta} = 0 \quad (13b)$$

where $\epsilon = A/H$, $\lambda_L = L/L_g$ and $r = C_D LA/H^2$. Here L_g is the tidal wave length \sqrt{gH}/σ . In the following the depth dependence of the bottom friction will be neglected.

The boundary conditions read

$$\zeta = \cos(t) + \beta \cos(2t + \phi) \quad \text{for } x = 0 \quad (14a)$$

$$u = 0 \quad \text{for } x = 1 \quad (14b)$$

The first boundary condition implies that an external tide is prescribed at $x = 0$, the entrance of the embayment, the second one requires the horizontal velocity to vanish at $x = 1$ (note that this is a different boundary condition from the one used in section 2).

It is assumed that the bed profile is known and is given by $h = 1 - (1 - x)^\alpha$ with $\alpha \geq 0$.

From now on, β , the amplitude of the external forcing is set to zero. Furthermore, the internally generated overtides are neglected ($\epsilon = 0$). The equations

become very simple, they read:

$$\zeta_t + [(1-h)u]_x = 0 \quad (15a)$$

$$u_t + \lambda_L^{-2} \zeta_x + ru = 0 \quad (15b)$$

with $\zeta = \cos(t)$ at $x = 0$ and $u_x < \infty$ at $x = 0$. This equation can be solved explicitly:

$$\zeta(x, t) = \frac{i}{A} \frac{\partial}{\partial x} \left\{ \sqrt{1-x} J_{\frac{1}{2-\alpha}} \left[\frac{2}{2-\alpha} \sqrt{\hat{L}} (1-x)^{\frac{2-\alpha}{2}} \right] \right\} e^{it} + \text{c.c} \quad (16a)$$

$$u(x, t) = \frac{1}{A} (1-x)^{\frac{1}{2}-\alpha} J_{\frac{1}{2-\alpha}} \left[\frac{2}{2-\alpha} \sqrt{\hat{L}} (1-x)^{\frac{2-\alpha}{2}} \right] e^{it} + \text{c.c} \quad (16b)$$

with

$$A = 2i \left. \frac{\partial}{\partial x} \right|_{x=0} \left\{ \sqrt{1-x} J_{\frac{1}{2-\alpha}} \left[\frac{2}{2-\alpha} \sqrt{\hat{L}} (1-x)^{\frac{2-\alpha}{2}} \right] \right\}$$

and

$$\hat{L} = \lambda_L^2 (1-ir) = \frac{\sigma^2 L^2}{gH} \left(1 - i \frac{C_D LA}{H^2} \right)$$

Note that $u(x,t)$ is zero only for $0 < \alpha < 1$ at $x = 1$, so this gives a restriction on the bed profiles that can be used to study in this simple model. Furthermore, note that $u_x \rightarrow \infty$ for all bed profiles, except for the flat bed $\alpha = 0$. This already indicates that it is not possible to use just any bed profile, but to show the dependence of resonance length on the bed profile, it is not essential.

In figure 10, the first resonance length is plotted as a function of α and C_D . If this figure is used for an estuary like the Westernscheldt, using the parameters as given in table 3, it is found that the resonance length of the Westernscheldt for the M_2 tide is $L_{\text{Res}}^{M_2} \sim 104\text{km}$. The next resonance length (for a flat bed profile at 3/4 of the tidal wave length) does not exist for the Westernscheldt, due the frictional damping (see figure 11). Note that, according to the model as described in section 2 in which the correct boundary conditions at the closed end are used and in which case the bed profile can adjust to a morphodynamic equilibrium profile, the first resonance length of an embayment like the Westernscheldt is approximately 120km.

One can conclude that the resonance length for fixed α decreases with increasing friction. Furthermore, it also decreases if α is increased from 0, a flat bed, to 1 (constantly sloping profile).

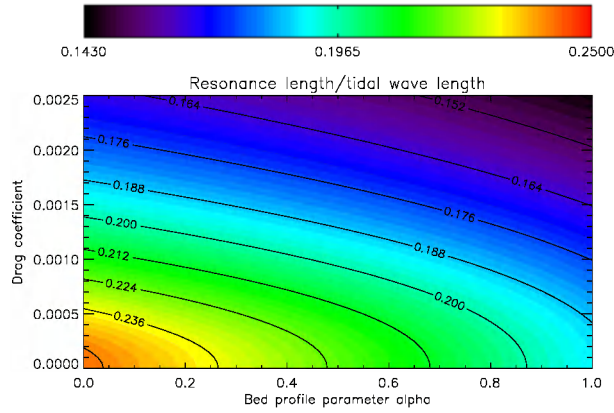


Figure 10: In this figure the resonance length compared to the tidal wave length $2\pi\sqrt{gH}/\sigma$, is plotted for different bed profiles (different α 's, where $h(x) = 1 - (1 - x)^\alpha$) and different values of drag coefficient C_D . Note that due to both friction and a depth dependent bed profile the resonance length becomes shorter.

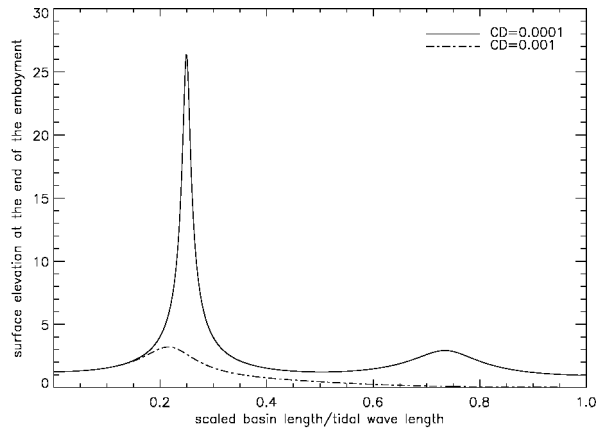


Figure 11: In this figure the amplitude of the vertical tide at the end of the embayment is plotted for two values of the drag coefficient C_D . For C_D small enough, more than one resonance length (with the length compared to the tidal wave length $2\pi\sqrt{gH}/\sigma$) is observed, if C_D is increased, only one resonance length is retained. Here $\alpha = 0$, but this observation is still valid for $\alpha > 0$.

B Frictional Length Scale

In this appendix, the frictional length scale for the M_2 -tide of an embayment is studied. The equations as derived in the previous appendix can be used.

Following Friedrichs & Madsen (1992), to calculate the frictional length scale, a spatially uniform water depth is chosen. Since this water depth has to be characteristic for the equilibrium, the maximum water depth h_{\min} is chosen in the continuity equation. A fraction of the maximum depth is chosen for the frictional contribution in the momentum equation since the choice of the maximum water depth underestimates the frictional strength at the end of the embayment considerably.

The equations now become:

$$\zeta_t + [h_{\min}u]_x = 0 \quad (17a)$$

$$u_t + \lambda_L^{-2}\zeta_x + \frac{ru}{\alpha h_{\min}} = 0 \quad (17b)$$

with α a constant between 0 and 1

Substituting $\exp(it)$ in the equations and combining them, a solution of the form $u(x=0)(1 - \exp(1-x)/\hat{L})$ can be found with a dimensionless frictional length scale defined by $L_f = 2\pi\Re(\hat{L})$. Since the embayment is only frictionally dominated at its end, this solution will probably only be valid near $x = 1$. After careful calculations, the frictional length scale reads

$$L_f = \frac{2\pi\sqrt{g\alpha h_{\min}H}}{\sigma L} \left[\frac{2}{1 + \sqrt{1 + \left(\frac{C_D AL}{\alpha h_{\min} H^2}\right)^2}} \right]^{\frac{1}{2}} \quad (18)$$

In ? it was shown that the maximum length of a short embayment is approximately L_f . If this observation and the results of the numerical experiments are used, it is found that the constant $\alpha \sim 0.39$. Now the maximum embayment length is reached when the friction length is approximately 1 (see table 4).

β	ϵ	L_{\max}	h_{\min}	x_{\min}	L_f/L_{\max}
0.0	0.067	242000	1.943	0.073	1.001
0.005	0.067	236000	1.868	0.0716	1.010
0.01	0.067	230000	1.796	0.0702	1.019
0.025	0.067	216000	1.601	0.0649	1.027
0.05	0.067	198000	1.346	0.0551	1.027
0.07429	0.067	182000	1.162	0.0444	1.044
0.07429	0.117	169000	1.542	0.0525	1.095
0.1	0.067	168000	1.024	0.0232	1.070

Table 4: Frictional length scales.

C The Moving Boundary

In this appendix, the boundary conditions at the moving boundary will be derived in section C.1. In the next section, these conditions are used to obtain the boundary conditions at a fixed point in space. This fixed point is defined as the point where the water depth is zero if the free surface elevation is zero, *i.e.* at $x = L$ (remember that the length L of the embayment was defined in such a way that the bed elevation $h(x = L) = H$).

C.1 Boundary Conditions at the Moving Boundary

For the water motion, the kinematic boundary condition is used. This condition requires the total derivative of the water depth to be zero when the water depth is zero (a water particle cannot escape from the free water surface):

$$\frac{d}{dt}(\zeta + H - h) = \zeta_t + u(\zeta + H - h)_x = 0 \quad \text{at } \zeta(\hat{x}, t) + H - h(\hat{x}) = 0 \quad (19)$$

Here it has been used that the time scale of bottom changes is much larger than the tidal period. Furthermore $\hat{x}(t)$ is the x -coordinate where the free water surface intersects the bed. Combining this condition with the continuity equation (1a) yields

$$(\zeta + H - h)u_x = 0 \quad \text{at } \zeta + H - h = 0 \quad (20)$$

Therefore, this kinematic boundary condition only requires u_x to be finite.

For the concentration one can require the Lagrangian flux to be zero at the free water surface, *i.e.* the sediment particles have the same Lagrangian velocity as the water particles:

$$(u - \hat{x}_t)C - \mu_* C_x = 0 \quad (21)$$

However, if one measures the flux at a fixed point in space, the net sediment flux is not zero. This phenomenon is called the Stokes drift (see Mei (1989)). This means that, if this boundary condition is accepted, a steady sediment flux towards or from the land is allowed.

If a sediment flux at the end of the embayment is not acceptable, one must correct for the Stokes drift. This means that one assumes that the velocity of a sediment particle and a water particle are not the same. The resulting boundary condition reads

$$[(u - \hat{x}_t)C - \mu_* C_x] - \text{Stokes Drift} = 0 \quad (22)$$

In dimensionless form, using the scaling as proposed in section 2, the boundary conditions read

$$(1 - h + \epsilon\zeta)u_x = 0 \quad \text{at } 1 - h + \epsilon\zeta = 0 \quad (23a)$$

$$\epsilon(u - \hat{x}_t)C - \mu_* C_x = 0 \quad (23b)$$

$$\text{or} \quad \text{at } 1 - h + \epsilon\zeta = 0 \quad (23c)$$

$$[\epsilon(u - \hat{x}_t)C - \mu_* C_x] - \text{Stokes Drift} = 0 \quad (23d)$$

In the text, the Eulerian no flux condition is used.

C.2 Boundary Conditions at a Fixed Space Coordinate

Using a Taylor expansion around a fixed coordinate, the boundary conditions on the moving boundary can be evaluated at a fixed space coordinate $x = 1$ where $h(x = 1) = 1$. Define $\epsilon\tilde{x}$ as the difference between the coordinate where $1 - h + \epsilon\zeta = 0$, \hat{x} , and $x = 1$. By making a Taylor expansion of the moving boundary around $x = 1$, one finds

$$1 - h + \epsilon\zeta = 1 - h|_{x=1} - \epsilon\tilde{x} h_x|_{x=1} - \frac{1}{2}\epsilon^2\tilde{x}^2 h_{xx}|_{x=1} + \epsilon\zeta|_{x=1} + \epsilon^2\tilde{x}\zeta_x|_{x=1} = 0$$

Expanding \tilde{x} and ζ in terms of the small parameter $\epsilon = A/H$, (hence $\tilde{x} = \tilde{x}^0 + \epsilon\tilde{x}^1 + \dots$, etc.), an expression for \tilde{x} can be found:

$$\tilde{x}^0 = \frac{\zeta^0}{h_x} \quad (24a)$$

$$\tilde{x}^1 = \frac{-\frac{1}{2}(\tilde{x}^0)^2 h_{xx} + \zeta_1 + \tilde{x}^0 \zeta_x^0}{h_x} \quad (24b)$$

By expressing the physical quantities at the moving boundary by a Taylor expansion around $x = 1$, one finds for u

$$u(1 - h + \epsilon\zeta) = u|_{x=1} + \epsilon\tilde{x} u_x|_{x=1} + \frac{1}{2}\epsilon^2\tilde{x}^2 u_{xx}|_{x=1} + \dots$$

Similar expansions can be derived for ζ and C .

By expanding u , ζ and C in the small parameter ϵ as well, the boundary conditions at the moving boundary can be completely expressed in terms of the physical quantities, evaluated at $x = 1$. Hence the kinematic boundary condition, evaluated at $x = 1$ and expanded in ϵ , reads

$$(1 - h)u_x^0 \text{ is finite} \xrightarrow{\text{using (5a)}} u^0 = \frac{\zeta_t^0}{h_x} \quad (25a)$$

$$(1 - h)u_x^1 + (1 - h)\frac{\zeta^0}{h_x}u_{xx}^0 \text{ is finite} \xrightarrow{\text{using (5a)}} u^1 = \frac{(\zeta^0 u^0)_x + \zeta_t^1}{h_x} \quad (25b)$$

where in the last step we have used that both u_x^1 and u_{xx}^0 have to be finite.

Of course, the velocity of a water particle at the free water surface is the same as the velocity of the free water surface itself. It is easily seen that u^0 and u^1 as defined in (25) are identical to $u^0 = x_t^0$ and $u^1 = x_t^1$.

The boundary condition (23c) becomes

$$\mu \left[C_x + \epsilon \frac{\zeta^0}{h_x} C_{xx} + \frac{1}{2}\epsilon^2 \frac{-\frac{1}{2}(\tilde{x}^0)^2 h_{xx} + \zeta_1 + \tilde{x}^0 \zeta_x^0}{h_x} C_{xxx} + \dots \right] \quad (26)$$

If (23d) is used, the boundary condition for the time-averaged flux becomes

$$\langle \epsilon u C - \mu C_x \rangle = 0 \quad (27)$$

while the time-varying fluxes still satisfy condition (26).

D Closure of the Eastern Scheldt

After severe floods in 1953 in the south of Holland, it was decided to protect the land by shortening the length of the coast-line of the Delta-area and increasing the height of the dikes (the so-called Delta Plan, see ?). Originally it was proposed to close all the tidal inlets by dams, except for the New Waterway and the Western Scheldt, the shipping routes to Rotterdam and Antwerp. However, due to an increase of environmental awareness in the 1970's, it was decided to keep the Eastern Scheldt open by building a moving barrier instead of a dam. In 1986 this storm-surge barrier was finished, containing many gates that can be closed in case of extreme high water.

The length of this embayment is approximately 45 km, its width 8 km and its depth at the entrance 20 m. Before closure the amplitude of the M_2 at the entrance of the embayment (measured at "Binnen Schaar", averaged over the year 1981) was approximately 1.35 m with $\phi_{M_2} = 74.5^\circ$, the amplitude of $M_4 \sim 0.11$ m with $\phi_{M_4} = 135.3^\circ$. After closure the amplitudes of M_2 decreased to 1.20 m with $\phi_{M_2} = 86.9^\circ$ and $M_4 \sim 0.04$ m with $\phi_{M_4} = 160.0^\circ$ (measured at "Binnen Schaar", averaged over the year 1989). Assuming that before the closure the system was in morphodynamic equilibrium, the system will not be in equilibrium anymore after closure. From observations and studies, it appears that the system is importing sediment.

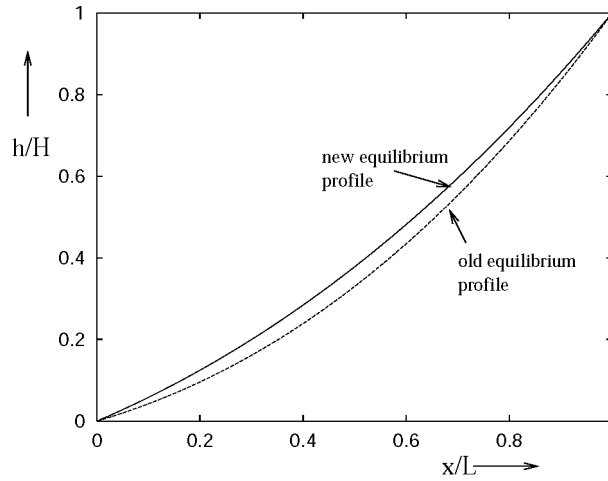


Figure 12: The equilibrium profiles for the Eastern Scheldt before and after the building of the storm surge. The embayment length $L = 45$ km, its depth at the entrance $H = 20$ m and its width 8 km. The area between the two equilibria is the total amount of sediment that has to be imported by the system to be able to reach this new equilibrium. Using this figure it is estimated to be $231 \times 10^6 \text{ m}^3$ of sediment.

Using the idealized model as described in section 2, an estimate of the deficit

of sediment can be made by assuming that the system will evolve towards its new equilibrium while its length does not change (in the Eastern Scheldt this is a good assumption since it is confined by the Oesterdam at its land side). In figure 12, the equilibrium before and after closure is shown. If the area between the two equilibria is integrated, the total amount of sediment deficit is found. This turns out to be $231 \times 10^6 \text{ m}^3$ of sediment. This is the correct order of magnitude compared with the estimated sand deficit of $400 \times 10^6 \text{ m}^3$. Considering the many simplifying assumptions underlying the model, this result is satisfactory.

References

- CSANADY, G.T. 1982. *Circulation in the coastal ocean*. Dordrecht: Reidel.
- DE JONG, K. 1998. *Tidally averaged transport models*. Ph.D. thesis, Delft University of Technology, The Netherlands.
- DE VRIEND, H. J. 1996. Mathematical modelling of meso-tidal barrier island coasts. Part I: Empirical and Semi-Emperical Models. *Pages 115–149 of: LIU, P.L.-F (ed), Advances in coastal and ocean engineering*. World Scientific, Singapore.
- DYER, K.R., & SOULSBY, R.L. 1988. Sand transport on the continental shelf. *Ann. Rev. Fluid Mech.*, **20**, 295–324.
- FOKKINK, R.J. 1998. *Morphodynamic network simulations of the Westerschelde*. report Z0919. Delft Hydraulics.
- FREDSOE, J., & DEIGAARD, R. 1992. *Mechanics of coastal sediment transport*. Singapore: World Scientific.
- FRIEDRICH, C.T. 1995. Stability shear stress and equilibrium cross-sectional geometry of sheltered tidal channels. *J. Coastal Res.*, **11**, 1062–1074.
- FRIEDRICH, C.T., & MADSEN, O.S. 1992. Nonlinear diffusion of the tidal signal in frictionally-dominated embayments. *J. Geophys. Res.*, **97**, 5637–5650.
- JEUKEN, M.C.J.L. 1998. *De functie en het gedrag van kortsluitgeulen in het westelijke deel van de Westerschelde*. report R98-06. Institute for Marine and Atmospheric Research, Utrecht University.
- LORENTZ, H.A. 1922. Het in rekening brengen van den weerstand bij schommelende vloeistofbewegingen. *De Ingenieur*, 695.
- MEI, C.C. 1989. *The applied dynamics of ocean surface waves*. Singapore: World Scientific.
- SCHUTTELAARS, H.M. 1997. *Evolution and stability analysis of bottom patterns in tidal embayments*. Ph.D. thesis, University of Utrecht, The Netherlands.
- SCHUTTELAARS, H.M., & DE SWART, H.E. 1996. An idealized long-term morphodynamic model of a tidal embayment. *Eur. J. Mech., B/Fluids*, **15**(1), 55–80.
- VAN DER SPEK, A.J. 1997. Tidal asymmetry and long-term evolution of Holocene tidal basins in The Netherlands, simulation of paleo-tides in the Schelde estuary. *Marine Geology*, **141**, 71–90.
- VAN RIJN, L.C. 1993. *Principles of sediment transport in rivers, estuaries and coastal seas*. Amsterdam: Aqua Publ.

- VERBEEK, H., TANK, F.T.G., & GROENEWOUD, M.D. 1998. *Drempels in de Westerschelde, natuur en mens samen aan het werk*. Tech. rept. RIKZ.
- ZIMMERMAN, J.T.F. 1982. On the Lorentz linearization of a quadratically damped forced oscillator. *Phys. Lett.*, **89A**, 123–124.
- ZIMMERMAN, J.T.F. 1992. On the Lorentz linearization of a nonlinearly damped tidal Helmholtz oscillator. *Proc. Kon. Ned. Akad. v. Wetensch.*, **95**, 127–145.